



UNIVERSITY OF LEEDS

This is a repository copy of *Superconductor derived from a topological insulator heterostructure*.

White Rose Research Online URL for this paper:  
<http://eprints.whiterose.ac.uk/130708/>

Version: Supplemental Material

---

**Article:**

Sasaki, S [orcid.org/0000-0002-8915-6735](https://orcid.org/0000-0002-8915-6735), Segawa, K and Ando, Y (2014) Superconductor derived from a topological insulator heterostructure. *Physical Review B - Condensed Matter and Materials Physics*, 90 (22). 220504(R). ISSN 1098-0121

<https://doi.org/10.1103/PhysRevB.90.220504>

---

**Reuse**

Items deposited in White Rose Research Online are protected by copyright, with all rights reserved unless indicated otherwise. They may be downloaded and/or printed for private study, or other acts as permitted by national copyright laws. The publisher or other rights holders may allow further reproduction and re-use of the full text version. This is indicated by the licence information on the White Rose Research Online record for the item.

**Takedown**

If you consider content in White Rose Research Online to be in breach of UK law, please notify us by emailing [eprints@whiterose.ac.uk](mailto:eprints@whiterose.ac.uk) including the URL of the record and the reason for the withdrawal request.



[eprints@whiterose.ac.uk](mailto:eprints@whiterose.ac.uk)  
<https://eprints.whiterose.ac.uk/>

# Supplemental Material for “New superconductor derived from topological insulator heterostructure”

Satoshi Sasaki,<sup>1</sup> Kouji Segawa,<sup>1</sup> and Yoichi Ando<sup>1</sup>

<sup>1</sup>*Institute of Scientific and Industrial Research,  
Osaka University, Ibaraki, Osaka 567-0047, Japan*

(Dated: August 15, 2014)

## Materials and methods

High-quality single crystals of  $(\text{PbSe})_5(\text{Bi}_2\text{Se}_3)_6$  (PSBS) were grown by a modified Bridgman method using high purity elements Pb (99.998%), Bi (99.9999%), and Se (99.999%) with the starting composition of Pb:Bi:Se = 7:26:46 (molar ratio) in a sealed evacuated quartz tube at 698 °C for 6 h, followed by a slow cooling to 650 °C with a cooling rate of 12 °C/day and then quenching to room temperature. Due to the phase diagram of the Pb-Bi-Se ternary system [1], the  $m = 1$  and 2 phases sequentially crystallize in a boule in the present self-flux-type growth. After the growth, we chose the  $m = 2$  PSBS phase based on the x-ray diffraction (XRD) analysis of the crystals cut out from the boule. Roughly 30% of a boule is in the  $m = 2$  PSBS phase. The starting composition has been optimized to yield reasonably large, single-phase crystals of the  $m = 2$  phase without detectable inclusions of the  $m = 1$  phase in the XRD analysis; note that the crystal quality has been greatly improved from that in Ref. [2]. The composition analysis using inductively-coupled plasma atomic emission spectroscopy (ICP-AES), which measures the averaged composition of a dissolved sample, supported the single-phase nature of the obtained  $m = 2$  crystals.

For the electrochemical Cu intercalation, we used a saturated solution of CuI powder (99.99%) in acetonitrile  $\text{CH}_3\text{CN}$  [3]. Samples with a typical size of  $2 \times 1 \times 0.2 \text{ mm}^3$  were wound by a 50- $\mu\text{m}$  thick, bare Cu wire, and they together acted as the working electrode. A 0.5-mm thick Cu stick was used as both the counter and reference electrode. The concentration of intercalated Cu was determined from the weight change before and after the intercalation process, giving the  $x$  value of  $\text{Cu}_x(\text{PbSe})_5(\text{Bi}_2\text{Se}_3)_6$  (CPSBS). The samples were then annealed in a sealed evacuated quartz tube at 550 °C for 2 h and quenched by dropping the quartz tube into cold water to activate the superconductivity. To confirm the validity of the Cu concentration  $x$  determined from the mass change, we have performed ICP-AES analyses on several samples after they are annealed. The results are shown in Table I, which also presents the compositions of three pristine PSBS crystals for comparison. The  $x$  values determined from the two methods agree within 10%.

The dc magnetic susceptibility was measured with a commercial SQUID magnetometer (Quantum Design MPMS-1); the remnant field was removed with the magnet reset procedure and the error in the applied field was less than 0.01 mT. The resistivity  $\rho_{xx}$  and the Hall

$x$ from mass	Cu	Pb	Bi	Pb+Bi	Se
				(fixed)	
0	0	3.24(11)	13.8(1)	17	23.7(1)
0	0	3.23(9)	13.8(1)	17	23.6(1)
0	0	3.12(8)	13.9(1)	17	23.5(1)
0.85	0.84(1)	3.11(12)	13.9(1)	17	23.4(1)
1.22	1.19(1)	3.22(9)	13.8(1)	17	23.7(2)
1.25	1.15(1)	3.09(12)	13.9(1)	17	23.6(1)
1.85	1.70(1)	3.19(10)	13.8(1)	17	23.7(1)

TABLE I: Results of the ICP-AES analyses. The nominal formula for  $m = 2$  is  $\text{Cu}_x\text{Pb}_5\text{Bi}_{12}\text{Se}_{23}$ . Since the ICP-AES analysis only gives relative compositions of the constituent elements, we fixed the total cation composition of PSBS (i.e. Pb+Bi) to be 17 in this table. One can see that  $\text{Bi}_{\text{Pb}}^{\bullet}$  antisite defects naturally occur in PSBS crystals to cause a lot of  $n$ -type doping, which is partially compensated by excess Se. The Cu content is consistent with the  $x$  value determined from the mass change within 10%.

resistivity  $\rho_{yx}$  were measured by using a standard six-probe method where the contacts were made by attaching gold wires with a vacuum-cure silver paint. The Hall coefficient  $R_H$  was calculated from the slope of  $\rho_{yx}(B)$ . The specific heat  $c_p$  was measured with a relaxation-time method using a commercial equipment (Quantum Design PPMS-9). To confirm the reproducibility of the specific-heat data, we made detailed measurements on two superconducting samples with nearly 100% shielding fractions,  $x = 1.36$  and  $1.66$ , both of which had  $T_c = 2.85$  K.

### S1. Carrier density and Cu intercalation

Temperature dependencies of  $R_H$  in pristine PSBS and superconducting CPSBS ( $x = 1.36$ ) are shown in Fig. S1(a). The carrier density  $n_e$  is calculated from the value of  $R_H$  at 4 K, and it is  $4 \times 10^{20} \text{ cm}^{-3}$  in PSBS and  $1.2 \times 10^{21} \text{ cm}^{-3}$  in CPSBS. The magnetic-field dependence of  $\rho_{yx}$  in CPSBS at 4 K is essentially linear, indicating that only one type of electron carriers dominate the transport properties; namely, the physics is dominated by only one band. This suggests that the topological and nontopological bands of the  $\text{Bi}_2\text{Se}_3$  unit observed in PSBS [2] may well have merged at the chemical potential of CPSBS that has been raised due to the electron doping.

In CPSBS samples, the volume density of Cu atoms is given by  $n_{\text{Cu}} = x(d/M)N_A$ , where  $d = 7.715 \text{ g/cm}^3$  is the density of PSBS,  $M = 5359.8 \text{ g/mol}$  is the molar mass, and  $N_A$  is

the Avogadro constant. For  $x = 1.36$ , one obtains  $n_{\text{Cu}} = 1.18 \times 10^{21} \text{ cm}^{-3}$ . On the other hand, the increase in the electron carrier density upon Cu intercalation in this sample is given by  $\Delta n_e = (1.2 \times 10^{21}) - (4 \times 10^{20}) = 8 \times 10^{20} \text{ cm}^{-3}$ . Therefore, one can estimate that each intercalated Cu introduces  $\Delta n_e/n_{\text{Cu}} = 0.68$  electron on average, which is much more efficient than in  $\text{Cu}_x\text{Bi}_2\text{Se}_3$  [4]. In view of the report by Koski *et al.* [5] that zero-valent copper atoms can be present in the van der Waals gap of  $\text{Bi}_2\text{Se}_3$ , the less-than-100% efficiency of the intercalated Cu as a donor is probably due to its neutralization. Also, the variation in the shielding fractions shown in Fig. 1(d) of the main text may also be a reflection of the difficulty in controlling the valence state of intercalated Cu.

## S2. Specific heat analyses

The temperature dependence of the total specific heat  $c_p$ , which includes both the phononic and electronic contributions,  $c_{\text{ph}}$  and  $c_{\text{el}}$ , respectively, is shown in Fig. S2 for 0 and 2 T. The conventional Debye fitting using

$$c_p = c_{\text{el}} + c_{\text{ph}} = \gamma_{\text{N}}T + A_3T^3 + A_5T^5 \quad (1)$$

to the 2 T data, which represent mostly the normal-state behavior in the fitted temperature range, describes well the data up to 5 K. From this fitting we obtain the normal-state electronic specific-heat coefficient  $\gamma_{\text{N}} = 5.89 \text{ mJ/mol K}^2$ . Assuming that the system is quasi-2D, this  $\gamma_{\text{N}}$  corresponds to the effective mass  $m^* = (3\hbar^2c^*\gamma_{\text{N}})/(V_{\text{mol}}k_{\text{B}}^2) = 2.6m_e$ , where  $c^* = 5.06 \text{ nm}$  is the lattice constant along the  $c^*$  direction,  $V_{\text{mol}} = 694.7 \text{ cm}^3/\text{mol}$  is the molar volume, and  $m_e$  is the free electron mass. The coefficients of the phononic contribution are  $A_3 = 3.73 \text{ mJ/mol K}^4$  and  $A_5 = 0.10 \text{ mJ/mol K}^6$ , and the former gives the Debye temperature  $\theta_D = 153.1 \text{ K}$ .

We found that in high magnetic fields (above  $\sim 1.5 \text{ T}$ ), a Schottky anomaly becomes noticeable in the  $c_p(T)$  data at low temperature. We therefore analyzed the small Schottky

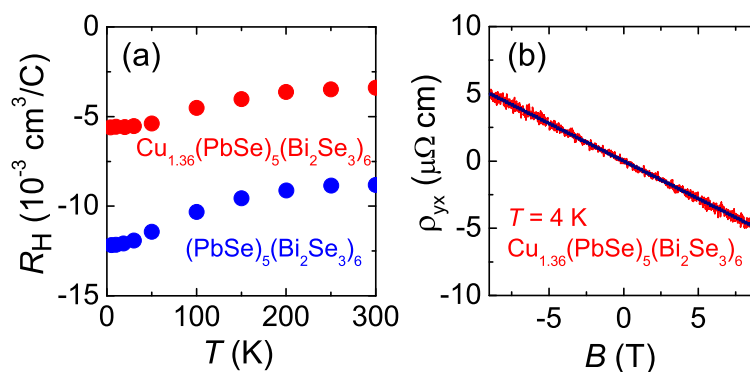


FIG. S1: (a) Temperature dependencies of the Hall coefficient  $R_{\text{H}}$  in pristine PSBS and superconducting CPSBS ( $x = 1.36$ ). (b) Magnetic-field dependence of  $\rho_{yx}$  measured in CPSBS ( $x = 1.36$ ) at 4 K. The solid line emphasizes the linear nature of the  $B$  dependence.

contribution  $c_{\text{Sch}} \equiv c_p - c_{\text{ph}} - c_{\text{el}}$  using the two-level Schottky model with free  $S = 1/2$  moments [6, 7],

$$c_{\text{Sch}}(T, B) = \frac{nx^2e^x}{(1+e^x)^2} \quad \left( x \equiv \frac{g\mu_B B}{k_B T} \right), \quad (2)$$

where  $g$  is the Landé  $g$  factor and  $n$  is a coefficient in the unit of the universal gas constant  $R$ . The temperature below which an upturn starts is determined solely by the  $g$  factor, which is found to be 0.17 from the data of the  $x = 1.36$  sample in high magnetic fields above  $B_{c2}$  [Fig. S3(c)]; such a small  $g$  factor has been reported to come from an anisotropy caused by crystal fields [8–11] or from hyperfine-enhanced nuclear magnetic moments [12, 13]. The upturns in the 2 – 5 T data shown in Figs. S3(a) and S3(c) are consistently reproduced by Eq. (2) with the coefficient  $n = 3.1$  mJ/mol K, which corresponds to the free-moment concentration of only  $\sim 0.037\%$ . It is worth emphasizing that the superconductivity in CPSBS is already suppressed above  $\sim 2$  T at 0.35 K, so the observed Schottky anomaly is largely irrelevant when one discusses the specific-heat behavior in the superconducting state. The calculated curves in Fig. S3(b) show that the peak due to this Schottky anomaly is expected to occur at a much lower temperature than our experimental range.

To gain insight into the origin of this small Schottky anomaly, we have measured the normal-state magnetic susceptibilities  $\chi_{\perp}$  and  $\chi_{\parallel}$  for  $B \perp ab$  and  $B \parallel ab$ , respectively, down to the lowest temperature of our SQUID magnetometer, 1.8 K. The result is shown in Fig. S4, where one can see that there is no visible Curie behavior in neither of the field directions. If the Schottky anomaly was due to  $\sim 0.037\%$  of  $S = 1/2$  free electron spins that happen to have a small  $g$  factor for  $B \perp ab$  due to crystal fields, they should give rise to a visible Curie behavior for  $B \parallel ab$  above 1.8 K, but we did not observe it. Therefore, one may conclude that the observed small Schottky anomaly is likely to be due to hyperfine-

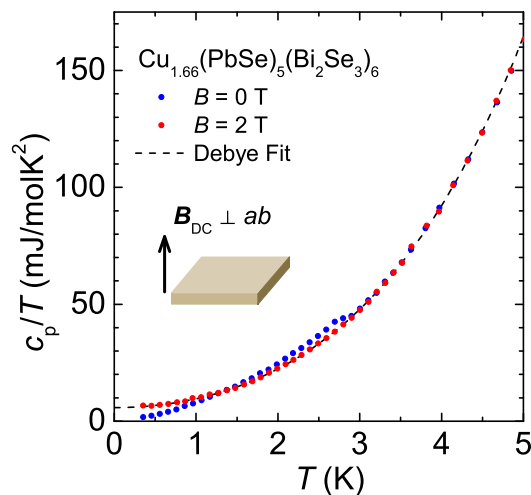


FIG. S2:  $c_p/T$  vs  $T$  data measured in 0 and 2 T applied perpendicular to the  $ab$  plane. The dashed line is the Debye fitting to the 2-T data.

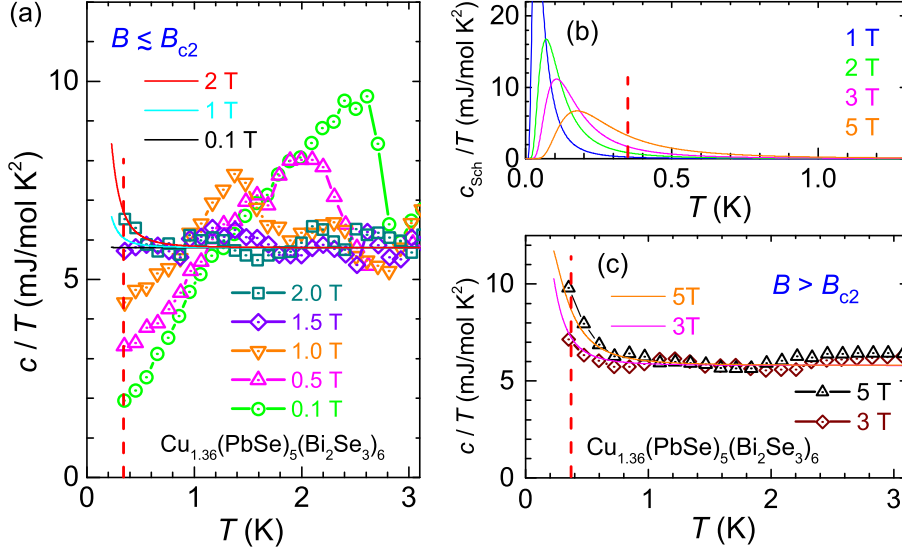


FIG. S3: Schottky anomaly in the  $x = 1.36$  sample. (a)  $(c_p - c_{\text{ph}})/T$  vs  $T$  data for  $B \lesssim B_{c2}$  (symbols), together with the calculated  $c_{\text{Sch}}/T + \gamma_N$  for  $B = 0.1, 1,$  and  $2$  T (solid lines). (b) Theoretical curves of the expected Schottky contribution  $c_{\text{Sch}}/T$  coming from  $0.037\%$  of  $S = 1/2$  moments with the Landé  $g$  factor of  $0.17$ . Those parameters are determined to consistently reproduce the data for the  $x = 1.36$  sample in  $2 - 5$  T. (c)  $(c_p - c_{\text{ph}})/T$  vs  $T$  data for  $B > B_{c2}$  and the calculated  $c_{\text{Sch}}/T + \gamma_N$  for  $B = 3$  and  $5$  T (solid lines). In panels (a)-(c), vertical red dashed lines mark the lowest experimental temperature.

enhanced nuclear magnetic moments, which originate from a minority valence state or a minority isotope of the constituent elements of CPSBS, or from some impurities that may have entered into the samples during the Cu intercalation process. However, it is difficult to name the actual element/isotope, because various nuclei can have hyperfine-enhanced moments and the concentration of the nucleus in question is only  $\sim 0.037\%$ . In any case, the determination of the exact source of the weak Schottky anomaly is not very important for the present study, as long as its contribution can be duly subtracted.

To make our best effort to quantify the magnetic-field dependence of  $c_{\text{el}}$  in the superconducting state, we calculated  $c_{\text{Sch}}(T, B)$  (which is only  $\lesssim 20\%$  of  $c_{\text{el}}$  at  $0.35$  K in  $2$  T and is negligible in  $1$  T) and subtracted it from all the specific-heat data in magnetic fields. The  $c_{\text{el}}/T$  vs  $T$  data measured in the  $x = 1.36$  sample in various magnetic fields applied perpendicular to the  $ab$  plane are shown in Fig. S5(a) after the subtraction of  $c_{\text{Sch}}(T, B)/T$ ; for comparison, Fig. S3(a) shows the data for  $(c_p - c_{\text{ph}})/T$  before subtraction of  $c_{\text{Sch}}/T$ , as well as the calculated Schottky component in terms of  $c_{\text{Sch}}(T, B)/T + \gamma_N$  for selected field values. The  $c_{\text{el}}(B)$  behavior at  $0.35$  K for this sample is shown in Fig. S5(b), which is best described with  $c_{\text{el}} \sim B^{0.56}$ ; in this figure, we also show the uncorrected  $c_{\text{el}}(B)$  data including

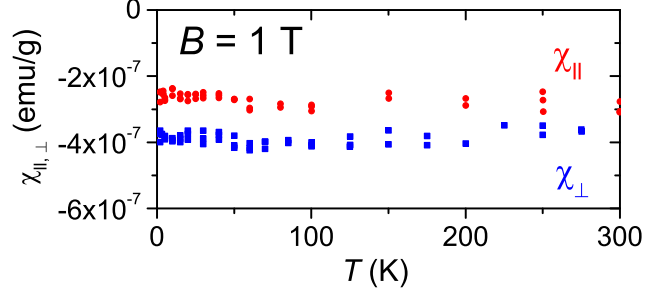


FIG. S4: Normal-state magnetic susceptibilities  $\chi_{\perp}$  and  $\chi_{\parallel}$  measured on the  $x = 1.66$  sample down to 1.8 K in 1 T applied perpendicular and parallel to the  $ab$  plane, respectively.

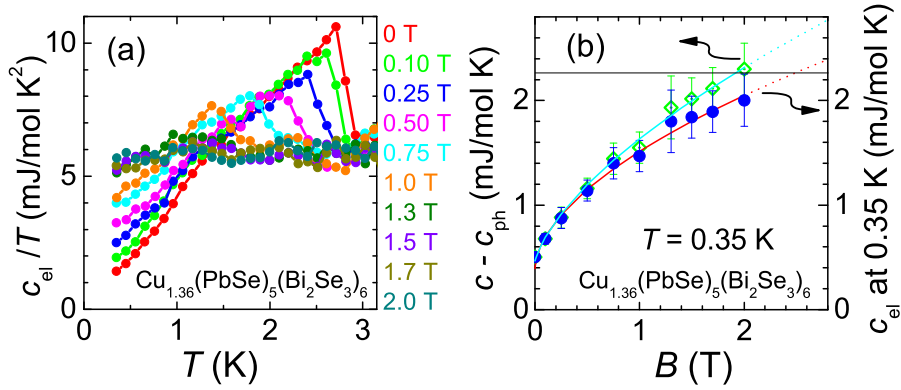


FIG. S5: (a)  $c_{\text{el}}/T$  vs  $T$  plots for various magnetic fields ( $B \perp ab$ ) after subtracting the small Schottky contribution in CPSBS ( $x = 1.36$ ). (b) Magnetic-field dependence of  $c_{\text{el}}$  at 0.35 K taken from the data shown in (a). The red solid line is the best fit of the function  $aB^n + c_0$  to the data and gives  $n = 0.56 \pm 0.06$ ,  $a = 1.12 \pm 0.06 \text{ mJ mol}^{-1} \text{ K}^{-1} \text{ T}^{-n}$ , and  $c_0 = 0.39 \pm 0.05 \text{ mJ mol}^{-1} \text{ K}^{-1}$ . For comparison, we also show with light-green diamonds the  $B$  dependence of  $c - c_{\text{ph}}$  at 0.35 K without subtracting the Schottky contribution; the light-blue solid line is the best fit of the same function, yielding  $n = 0.63 \pm 0.06$ ,  $a = 1.3 \pm 0.1 \text{ mJ mol}^{-1} \text{ K}^{-1} \text{ T}^{-n}$ , and  $c_0 = 0.4 \pm 0.5 \text{ mJ mol}^{-1} \text{ K}^{-1}$ . Horizontal solid line corresponds to  $\gamma_{\text{N}}T$  at  $T = 0.35 \text{ K}$ .

the Schottky contribution, the effect of which does not qualitatively change the behavior. The power 0.56 obtained for  $c_{\text{el}}(B)$  is consistent with the result for the  $x = 1.66$  sample shown in the main text [Fig. 3(b)]. The parameters of the Schottky contribution used for obtaining the  $c_{\text{el}}/T$  data for the  $x = 1.66$  sample shown in Fig. 3(a) of the main text were the same as those for the  $x = 1.36$  sample.

As one can see in Fig. S5(a), the  $c_{\text{el}}/T$  vs  $T$  behavior broadens significantly in high

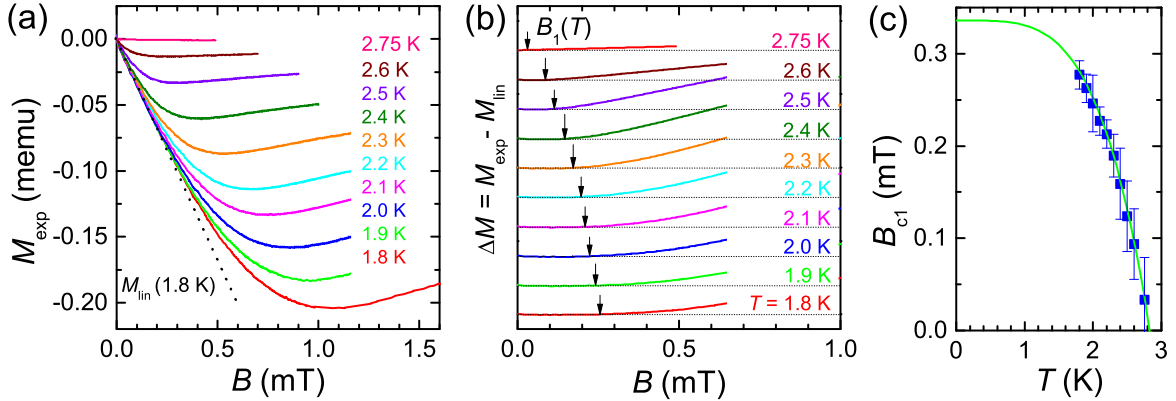


FIG. S6: (a) Initial  $M(B)$  behavior of the  $x = 1.66$  sample after zero-field cooling to various temperatures. (b) Plots of  $\Delta M \equiv M - aB$ , where  $a$  is the initial slope, together with the determination of  $B_1$  shown by arrows. (c)  $B_{c1\parallel}$  vs.  $T$  phase diagram; the solid line is a fit to the empirical formula shown in the text.

magnetic fields above  $\sim 1$  T, which makes it impossible to determine the mid-point of the specific-heat jump. We therefore try to extract the information about  $B_{c2}$  from  $c_{el}/T$  by determining, with a certain error bar, the onset temperature below which  $c_{el}/T$  deviates from  $\gamma_N$ , and such data are plotted in Fig. 4(b) of the main text.

### S3. Superconducting parameters

Figure S6 summarizes the results of the magnetization measurements of the  $x = 1.66$  sample to determine the lower critical field  $B_{c1}$ . Figure S6(a) shows  $M(B)$  curves measured after zero-field cooling to various temperatures in magnetic field applied parallel to the  $ab$  plane. We define  $B_1$  at each temperature as the value at which the  $M(B)$  data deviates from its initial linear behavior, as can be seen in Fig. S6(b). To obtain  $B_{c1\parallel}$ , those  $B_1$  values are corrected for the demagnetization effect, though it is small for  $B\parallel ab$ : Using the approximation given for the slab geometry [14], we obtain  $B_{c1\parallel} = B_1/\tanh\sqrt{0.36b/a}$ , with the aspect ratio  $b/a = 1.6/0.23$  in the present case. The resulting  $B_{c1\parallel}$  values are shown in Fig. S6(c). To determine the 0-K limit, we used the empirical formula  $B_{c1}(T) = B_{c1}(0)[1 - (T/T_c)^4]$  [15] and obtained  $B_{c1\parallel}(0) = 0.34$  mT. Note that the flux pinning in the present system is weak as evidenced by the small magnetic hysteresis [Fig. S7], which supports the reliability of the determination of  $B_{c1}$  using the above method [16].

From  $B_{c2\perp} = 2.6$  T, the coherence length  $\xi_{ab} = \sqrt{\Phi_0/(2\pi B_{c2\perp})} = 11.3$  nm is obtained, while from  $B_{c2\parallel} = 4.3$  T, we use  $\xi_{ab}\xi_{c^*} = \Phi_0/(2\pi B_{c2\parallel})$  and obtain  $\xi_{c^*} = 6.8$  nm. The anisotropy ratio is calculated as  $\gamma = B_{c2\parallel}/B_{c2\perp} = \lambda_{c^*}/\lambda_{ab} = 1.65$ ; here,  $\lambda_{c^*}$  and  $\lambda_{ab}$  are the penetration depths along the  $c^*$  and  $ab$  directions, respectively. Since we have the  $B_{c1}$  value only for  $B\parallel ab$ , we define the effective GL parameter  $\kappa_{ab} \equiv \sqrt{\lambda_{ab}\lambda_{c^*}/\xi_{ab}\xi_{c^*}}$  and use  $B_{c1\parallel} = \Phi_0 \ln \kappa_{ab}/(4\pi\lambda_{ab}\lambda_{c^*})$  together with  $B_{c2\parallel}/B_{c1\parallel} = 2\kappa_{ab}^2/(\ln \kappa_{ab} + 0.5)$  [17, 18] to obtain

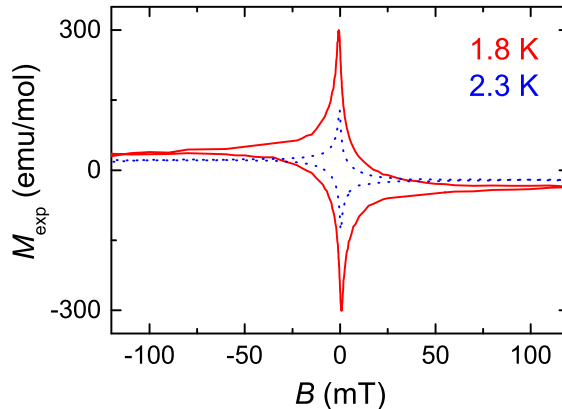


FIG. S7:  $M(B)$  curves measured on the  $x = 1.66$  sample at 1.8 and 2.3 K after subtracting the diamagnetic background.

$\kappa_{ab} \approx 192$ . We then obtain the thermodynamic critical field  $B_c = \sqrt{B_{c1\parallel} B_{c2\parallel}} / \ln \kappa_{ab} = 16.6$  mT and the penetration depths  $\lambda_{ab} = \kappa_{ab} \sqrt{\xi_{ab} \xi_{c^*}} / \gamma = 1.3 \mu\text{m}$  and  $\lambda_{c^*} = 2.2 \mu\text{m}$ .

#### S4. Characterization of the inhomogeneity

To characterize the nature of the inhomogeneity in CPSBS samples, we have measured the magnetization and specific heat of two samples, one ( $x = 1.07$ ) with the shielding fraction of 39% and the other ( $x = 0.96$ ) with the shielding fraction of only 15%. As shown in Fig. S8, the superconducting volume fraction inferred from the specific-heat data reasonably scales with the shielding fraction estimated from the magnetization. The observed scaling confirms that the shielding fraction is indeed a good measure of the superconducting (SC) volume fraction and that the SC part is not forming a “shell” to wrap the nonsuperconducting (NSC) part in CPSBS samples.

It is useful to note that even the electronic specific-heat coefficient  $\gamma$  in the normal state ( $\gamma_N$ ) changes systematically with the shielding fraction. This is natural, since the NSC part of the sample does not obtain the additional carriers from intercalated Cu and is expected to contain a relatively low carrier concentration ( $4 \times 10^{20} \text{ cm}^{-3}$ ), while the SC part of the sample has a higher carrier concentration ( $1.2 \times 10^{21} \text{ cm}^{-3}$ ), and hence the density of states of the two should be different; from the data in Fig. 2(d), the  $\gamma$  value for the SC parts is obtained to be  $6.4 \text{ mJ/mol K}^2$ , and the  $\gamma$  value of  $1.9 \text{ mJ/mol K}^2$  for the NSC part makes the estimate of the superconducting volume fraction based on the specific-heat data [Figs. S8(b) and S8(d)] to become consistent with the shielding fraction obtained from the magnetization data [Figs. S8(a) and S8(c)].

Furthermore, to remove the concern that the large observed shielding fraction might be due to surface superconductivity, we have performed an experiment to compare the shielding fractions before and after removing the surface layer of a sample with 94.6% shielding fraction. Since the CPSBS samples become rather brittle and difficult to cleave after the

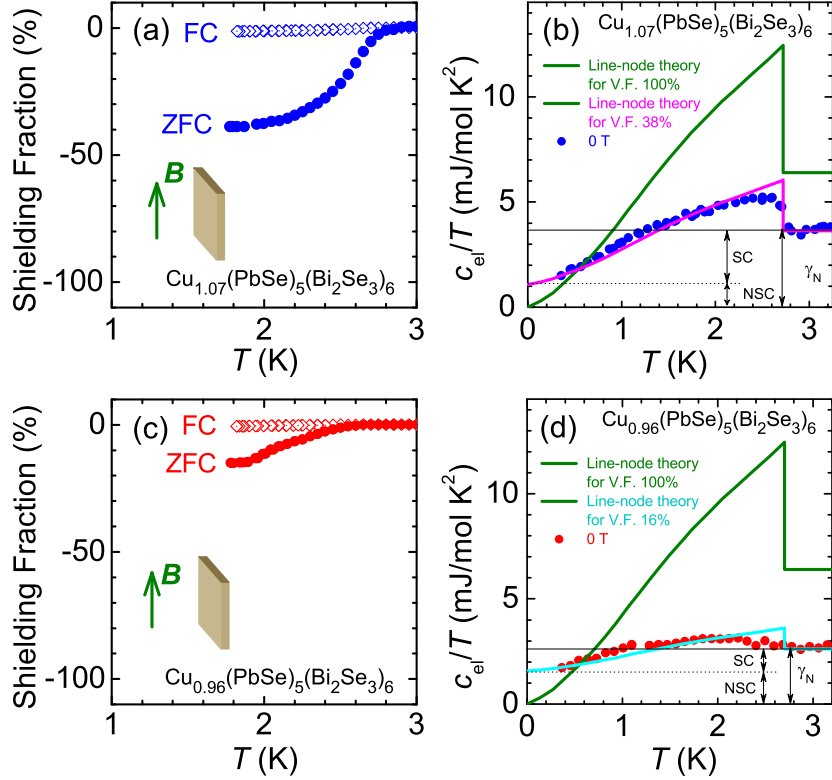


FIG. S8: (a) and (c) Temperature dependencies of the shielding fraction measured in 0.2 mT applied parallel to the  $ab$  plane for samples with (a)  $x = 1.07$  and (c)  $x = 0.96$ , both of which present relatively poor superconducting properties. (b) and (d) Superconducting transition in  $c_{el}/T$  in 0 T obtained for the two samples after subtracting the phonon contribution determined in 2 T. The green line is the theoretical curve for  $d$ -wave pairing with line nodes [19] with 100% SC volume fraction (V.F.), which has been shown in the main text [Fig. 2(d)] to reproduce the  $c_{el}/T$  data of the 100%-shielding-fraction sample reasonably well. The magenta and cyan lines show expected  $c_{el}/T$  behavior for a mixture of SC and NSC phases having  $\gamma$  of 6.4 and 1.9 mJ/mol K<sup>2</sup>, respectively, with the fraction of the former specified in the caption.

Cu intercalation, we gently filed off the top and bottom surfaces of a platelet-shaped sample using a sand paper; the weight of the sample was reduced from 1.00 mg to 0.955 mg after filing off the as-annealed surfaces. As shown in Fig. S9, the shielding fraction changed only a little, to 92.4%, after the filing. We suspect that this small reduction in the shielding fraction is due to a thin dead layer at the filed surface in which the superconducting property is weakened by the mechanical damage. In any case, this result precludes the possibility that

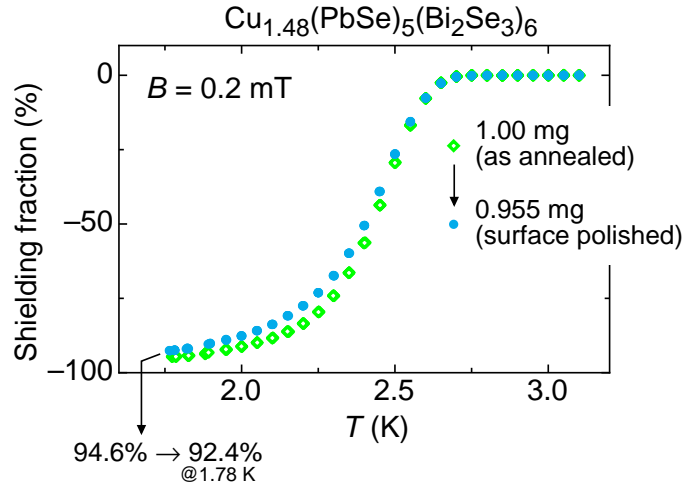


FIG. S9: Temperature dependencies of the shielding fraction measured in 0.2 mT applied parallel to the  $ab$  plane for a samples with  $x = 1.48$  before and after filing off the surface.

the large shielding fraction is due to surface superconductivity.

- 
- [1] L. E. Shelimova, O. G. Karpinskii, V. S. Zemskov, *Inorg. Mater. (USSR)* **44**, 927 (2008).
  - [2] K. Nakayama, K. Eto, Y. Tanaka, T. Sato, S. Souma, T. Takahashi, K. Segawa, and Y. Ando, *Phys. Rev. Lett.* **109**, 236804 (2012).
  - [3] M. Kriener, K. Segawa, Z. Ren, S. Sasaki, S. Wada, S. Kuwabata, and Y. Ando, *Phys. Rev. B* **84**, 054513 (2011).
  - [4] Y. S. Hor *et al.*, *Phys. Rev. Lett.* **104**, 057001 (2010).
  - [5] K. J. Koski *et al.*, *J. Am. Chem. Soc.* **134**, 7584 (2012)
  - [6] J. P. Emerson, R. A. Fisher, N. E. Phillips, D. A. Wright, E. M. McCarron III, *Phys. Rev. B* **49**, R9256 (1994).
  - [7] K. A. Moler *et al.*, *Phys. Rev. B* **55**, 3954 (1997).
  - [8] S. Holmes, D. K. Maude, M. L. Williams, J. J. Harris, J. C. Portal, K. W. J. Barnham, C. T. Foxon, *Semicond. Sci. Technol.* **9**, 1549 (1994).
  - [9] R. M. Hannak, M. Oestreich, A. P. Heberle, W.W. Rühle, K. Köhler, *Solid State Comm.* **93**, 313 (1995).
  - [10] P. Le Jeune, D. Robart, X. Marie, T. Amand, M. Brousseau, J. Barrau, V. Kalevich, D.

- Rodichev, *Semicond. Sci. Technol.* **12**, 380 (1997).
- [11] H. P. van der Meulen *et al.*, *Physica C* **152**, 65 (1988).
- [12] K. Andres, E. Bucher, *J. Appl. Phys.* **42**, 1522 (1971).
- [13] R. Movshovich, M. Jaime, J. D. Thompson, C. Petrovic, Z. Fisk, P. G. Pagliuso, J. L. Sarrao, *Phys. Rev. Lett.* **86**, 5152 (2001).
- [14] E. H. Brandt, *Phys. Rev. B* **60**, 11939 (1999).
- [15] M. Kriener, K. Segawa, S. Sasaki, and Y. Ando *Phys. Rev. B* **86**, 180505(R) (2012).
- [16] M. Kriener, K. Segawa, Z. Ren, S. Sasaki, and Y. Ando, *Phys. Rev. Lett.* **106**, 127004 (2011).
- [17] Clem, J. R. Phenomenological theory of magnetic structure in the high-temperature superconductors. *Physica C* **162-164**, 1137-1142 (1989).
- [18] Hu, C.-R. Numerical constants for isolated vortices in superconductors. *Phys. Rev. B* **6**, 1756-1760 (1972).
- [19] H. Won and K. Maki, *Phys. Rev. B* **49**, 1397 (1994).